Fe–N–C Electrocatalyst and Its Electrode: Are We Talking about the Same Material?

Viktoriia Saveleva, Kavita Kumar, Pascal Theis, Nicole Segura Salas, Ulrike Kramm, Frédéric Jaouen, Frédéric Maillard, Pieter Glatzel

Fe-N-C electrocatalyst and its electrode: are we talking about the same material?

Viktoriia A. Saveleva[1], Kavita Kumar[2], Pascal Theis[3], Nicole Segura Salas[3], Ulrike I. Kramm[3], Frédéric Jaouen[4], Frédéric Maillard[2], Pieter Glatzel[1]*

[1] ESRF, The European Synchrotron, 71 Avenue des Martyrs, CS40220, 38043 Grenoble Cedex 9, France

[2] Univ. Grenoble Alpes, Univ. Savoie Mont Blanc, CNRS, Grenoble INP, LEPMI, 38000 Grenoble, France

[3] TU Darmstadt, Department of Chemistry, Catalysts and Electrocatalysts Group, Technical University of Darmstadt, Otto-Berndt-Str. 3, 64287 Darmstadt, Germany

[4]ICGM, Univ. Montpellier, CNRS, ENSCM, Montpellier, France

KEYWORDS. Electrocatalyst, X-ray absorption spectroscopy, X-ray emission spectroscopy, catalyst layer, Fe-N-C.

ABSTRACT. Evaluation of the electrocatalyst performance data includes an electrode preparation step. Herein, we compare the structural composition of Fe-N-C materials, used to electrocatalyze the oxygen reduction reaction in proton-exchange membrane fuel cells, before and after catalyst

layer preparation. The effects of this step on the electronic structure and local coordination of Fe were investigated by X-ray absorption (XAS) and emission spectroscopies (XES), for Fe-N-C materials prepared via different synthetic routes. This work underlines the importance of determining the Fe-N-C catalyst structure in the prepared electrode for further studies of the structure – activity – stability correlations.

TEXT

The preparation of a homogeneous catalyst layer (CL) for electrochemical testing in either a rotating disc electrode (RDE) or in fuel cell set-up is a critical step. The CL of state-of-the-art polymer electrolyte fuel cells is a multi-phase medium comprising a catalyst, ionomer and pores. While a considerable amount of work has already been devoted to the preparation and analysis of Pt-based electrodes[1], similar studies on Pt-free materials, such as iron-nitrogen-carbon (Fe-N-C) catalysts, one of the most promising materials for acid and alkaline fuel cells, are less common.[2–4] Fe-N-C electrocatalysts are known to possess a complex composition containing typically several FeN_xC_y moieties (single Fe atoms coordinated to N atoms embedded into a C matrix) of different geometry, where the synthesis protocol favors the presence of certain FeN_xC_y sites and their amount.[5] Besides, Fe-N-C catalysts might also include Fe-based particles such as metallic Fe, Fe carbide or oxides.[6] The analysis of the structure of Fe atoms in Fe-N-C materials is often carried out using Mössbauer (MS) and/or X-ray absorption spectroscopies, where other complementary techniques such as electron microscopy, X-ray photoelectron spectroscopy, Raman spectroscopy are used for further characterization of the material both *ex situ*[7,8] and *in situ*/*operando*.[9–11] In general, the research related to Fe-N-C catalysts is focused either on the correlations between catalyst activity and its structure defined *ex situ*, or on the analysis of catalyst behavior under

reaction conditions, *i.e*. *in situ*/*operando*. It is also known that some Fe-N-C materials are sensitive to their storage conditions (oxygen and water presence)[2,12,13] as well as to any physical and/or chemical treatment resulting in the electrochemical activity changes.[14,15] Thus, one may expect some differences in the catalyst structure for a pristine powder and for a CL prepared based on it. In fact, it has been observed in the Mössbauer analysis of Fe-N-C catalyst powders and their CLs that the ratio between different FeN_x sites was changed[2] and new Fe-based species developed, such as Fe-based oxides.[16]

In this work, we applied Fe Kβ high energy resolution fluorescence detected (HERFD) X-ray absorption near edge structure (XANES) and Kβ X-ray emission spectroscopy (XES) techniques to analyze the structure of Fe-N-C catalysts in the CLs, *i.e*. Fe-N-C-based electrodes, and as the pristine powders. Analysis of the XANES provides information on the coordination of the Fe atoms, whereas Kβ XES, comprised of $K\beta_{1,3}$ and Kβ' components, is sensitive to changes in the Fe total spin.[17,18] The XAS and XES measurements were performed at beamline ID26 of the European synchrotron (ESRF). The experimental details on the beamline set-up and spectra analysis are provided in the Supporting Information.

The catalysts analyzed in this work have been obtained via different preparations: Fe0.5 is a metal-organic framework (MOF)-derived material prepared via ramp pyrolysis synthesis (labeled as $Fe_{0.5}$RP in previous publications)[19]; C-PPy, is a polypyrrole-derived isotopically enriched ^{57}Fe-N-C;[20] additionally a non-pyrolysed carbon-supported porphyrin Porph/C_{prec} and a porphyrin-based catalyst Porph/C_{cat} are included, both related to FeTMPPCl (5,10,15,20-tetrakis(4-methoxyphenyl)-21H,23H-porphine iron (III) chloride) supported on carbon.[8] More details on the preparation procedures can be found in the Supporting Information. The final composition of the obtained Fe-N-C catalysts strongly depends on their synthesis. On the basis of

previous data of low- and room-temperature Mössbauer spectroscopy, one can describe the materials with respect to their Fe-related compositions as follows: Porph/C_{prec} contains only porphyrin-like FeN_4 environments with an axial (chlorine) ligand,[8] both Fe0.5[5] and Porph/C_{cat} might be dominated by FeN_xC_y moieties, whereas C-PPy represents a mixture of molecular FeN_xC_y sites and crystalline or amorphous side phases.[8,10]

The Fe Kβ HERFD XANES and XES spectra recorded on the catalysts powders are shown in Figure 1 and Figure S1. XANES signatures of all analyzed catalysts possess characteristic features generally attributed to the FeN_xC_y sites.[5,11] The energy of the first inflection point of the Fe K edge is increasing in the following order: Porph/C_{prec} (7122.6 eV) < Fe0.5 (7123.9 eV) < C-PPy (7124.8 eV) < Porph/C_{cat} (7125.6 eV). Taking into account that the edge position is affected by several factors, *i.e*. Fe coordination number (CN), coordinated ligand nature and Fe valence, discrimination between Fe^{2+} and Fe^{3+} cannot be done only based on the position of Fe K edge.[21] For comparison, the first inflection point for Fe_2O_3 (with majority of Fe^{3+}) is at 7122.4 eV, lower than the position of the first inflection point for some of the studied catalysts, that are known to be a mixture of Fe^{2+} and Fe^{3+} oxidation states. This can be explained with the different ligand nature (oxygen / nitrogen / carbon / chlorine) and Fe coordination[22] without invoking a change in average oxidation state of iron atoms. The pre-edge and rising edge features at ≈ 7114 eV and 7119 eV, respectively, are sensitive to the Fe local geometry and its electronic structure. The rising edge (≈ 7119 eV) is characteristic of centro-symmetric square-planar (D_{4h}) Fe^{2+} components[11,23] and is well pronounced for Fe0.5, C-PPy and Porph/C_{cat}, however it is absent in the case of Porph/C_{prec} containing mostly 5-fold coordinated Fe sites. Considering FeN_4 molecular environments present in the catalysts Fe0.5, C-PPy and Porph/C_{cat}, the pre-edge peak (≈ 7114 eV) is assigned to 4-fold Fe^{2+} or Fe^{3+} coordinated environment of the FeN_xC_y sites.[24]

Interestingly, the pre-edge position of square-pyramidal (C_{4v}) sites of Porph/C_{prec} is at the same position, while its intensity is slightly higher than for Porph/C_{cat} (Figure S1) due to its noncentrosymmetric environment.[24] It should be noted, that a pre-edge feature is also found for iron oxide clusters (FeO_4 and FeO_5) in Al_2O_3 host structures, that show a magnetic ordering in Mössbauer spectroscopy only upon cooling to 3K.[25] Thus, iron oxide clusters that might be present to some extent in the catalyst, would give rise to a similar feature at (≈ 7114 eV). No significant difference in the Kβ spectra of the catalysts powders is observed indicating that the total spin on Fe does not change.

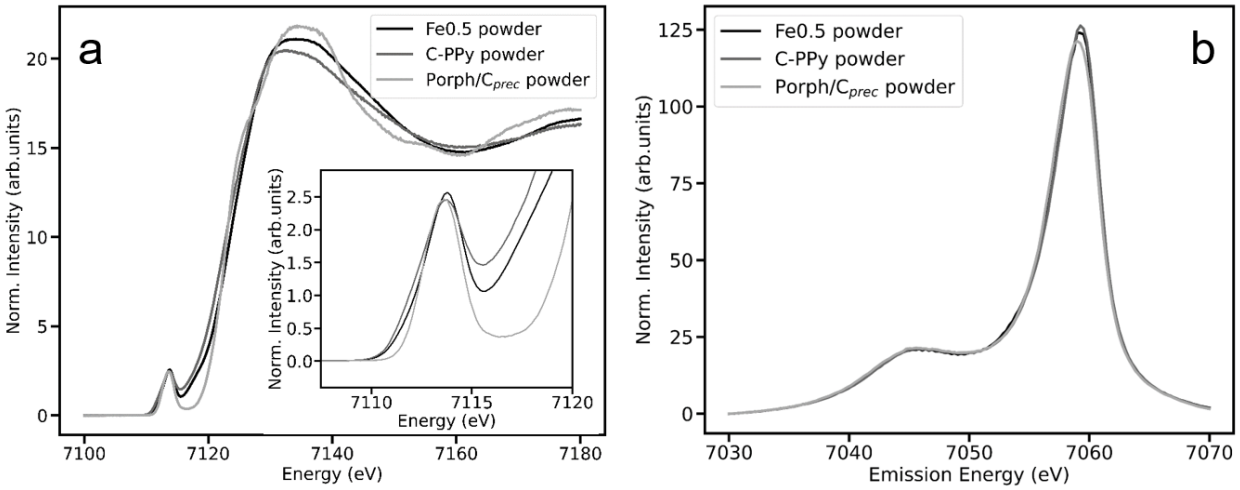

Figure 1. Fe Kβ HERFD XANES (a) and XES (b) spectra recorded on Fe-N-C catalyst powders. The pre-edge region is shown in the inset of panel a.

Next, we compare the XANES and XES signatures of the Fe-N-C powders and their CLs (Figure 2, Figure S1). The ink recipe and the overall electrode preparation procedure are described for each catalyst in detail in the Supporting Information. One can clearly see changes in the pre-edge region and in the white line (WL) of the Fe K edge as well as in Kβ emission line for the Fe-N-C-based electrodes in comparison to pristine powders. For all materials, we observe qualitatively the same trends when going from catalyst powder to theirs CLs: (i) increase in the WL intensity for

both peaks at ≈ 7131 eV and ≈ 7139 eV; (ii) shift of the Fe K edge position towards higher energies; (iii) decrease of the pre-edge peaks intensity (insets of Figure 2 and Figure S1); (iv) higher low-energy component of Kβ, Kβ', intensity and (v) blue shift of the Kβ mainline. Interestingly, the magnitude of change differs for the various catalysts. Porph/C_{prec} and Porph/C_{cat} (Figure 2c and Figure S1) seem to be least affected by the CL preparation procedure, whereas Fe0.5 shows the largest changes both in the XANES and XES data.

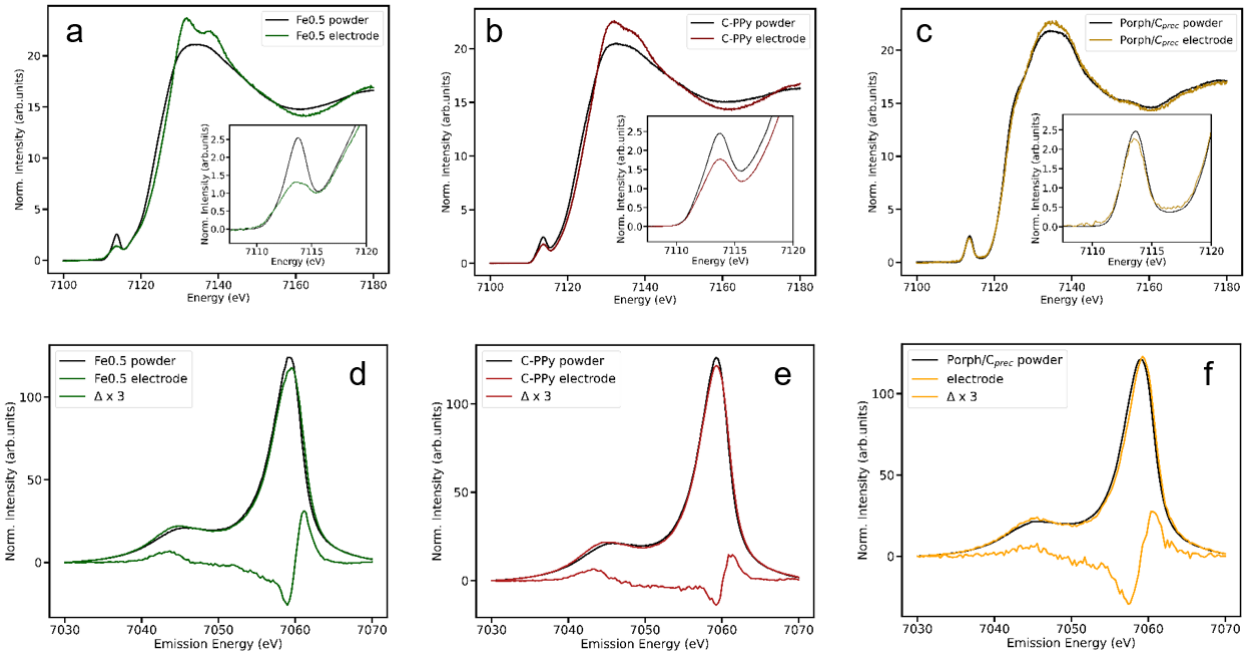

Figure 2. Comparison of Fe Kβ HERFD XANES (a-c) and XES (d-f) data obtained on the catalysts powders and their electrodes: for Fe0.5 (left), C-PPy (middle) and Porph/C_{prec} (right). Pre-edge regions are shown in the insets of the corresponding panels. Magnified Fe Kβ difference signals (Δ) for powder and electrode are shown in the bottom of the panels d-f.

The production of the CLs includes the preparation of the ink, followed by deposition of an aliquot on a conductive substrate. Typical substrates are glassy carbon (GC) electrodes, gas diffusion layers (GDLs), membranes etc. For more details on the design of the Pt-free CL the reader is therefore referred to a comprehensive review.[4] Composition of the catalyst inks used in

this work for preparing Fe-N-C-based CLs are listed in Table S2 and included water, isopropanol and Nafion® solution (which itself contains water, ethanol and isopropanol). Previously, Artyushkova *et al*. demonstrated a strong interaction of Nafion ionomer with an Fe-N-C catalyst in the CL, where the former was influenced by the catalyst structure.[3] Also Kramm *et al.* found a significant difference in absorption behavior for the as-prepared CL compared to the Fe-N-C catalyst.[2] Based on these and other studies[26,27], the influence of the Nafion-to-catalyst ratio (NCR) on the resulting Fe-N-C structure in the prepared electrodes was investigated by analyzing their spectroscopic signals. As the changes in the XANES and XES spectra are qualitatively similar for all the catalysts discussed in this work, we selected MOF-based catalyst Fe0.5 for this NCR study as it shows the most significant changes (see Figure 2). Figure 3 presents Fe K edge and Fe Kβ spectra for Fe0.5 powder and its CLs with the following NCR ratios: 0; 0.25; 0.5; 1 and 2. The increase of Nafion content from 0 to 2 results in a gradual shift of the Fe K edge, decrease of the pre-edge peak and growth of the white line as well as increase of Kβ' peak intensity accompanied with Kβ mainline shift towards higher emission energies (Table 1). Interestingly, we observe the same changes but less pronounced in the CL prepared from Nafion-free ink. In order to avoid any artefacts due to a possible increase of temperature during the sonication process (possibly leading to changes of the catalyst structure[28]) the ultrasonic bath was kept cold by adding ice in the case of C-PPy- and porphyrin-based inks or by using fridge stored water for Fe0.5-based inks (see Supporting Information).

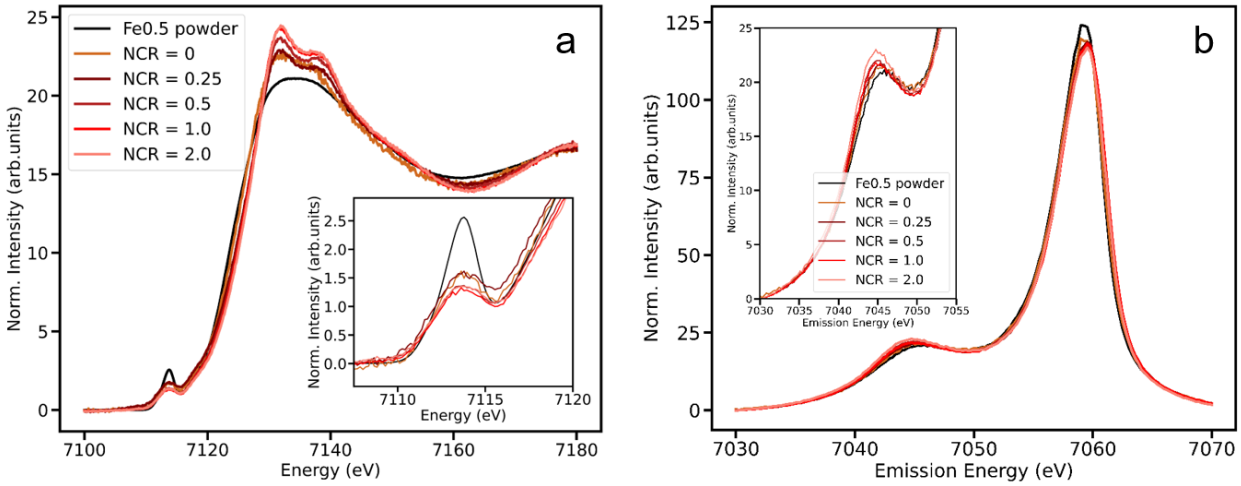

Figure 3. Fe Kβ HERFD XANES (a) and XES (b) spectra recorded on Fe0.5 catalyst powder and its electrodes with various NCR ratio. The insets show magnified pre-edge (a) and Kβ' (b) regions.

Next, we discuss the possible reasons for the observed spectral changes (summarized in Table 1) taking place during or after CL preparation as well as the role of Nafion in the CL. XANES spectra are affected by the local structure (bond distances and angles), ligand nature and oxidation state, where several descriptors define each spectral feature.[21] The pre-edge region spectral shape depends on the number of electrons in the *d*-shell, where its centroid and peak shape are sensitive to the oxidation state of Fe, while the pre-edge intensity is proportional to the amount of $3d - 4p$ hybridization, *i.e.* it is sensitive to site symmetry. The decrease in the peak intensity at ≈ 7114 eV, observed for all CLs studied here compared to the catalyst powders (Table 1), can be explained by an increase of the Fe coordination number via a square planar (D_{4h}) → octahedral (O_h) transition in case of Fe0.5, C-PPy catalysts and square pyramidal (C_{4v}) → O_h for Porph/C_{prec} material by formation of iron-oxygen/hydroxide bonds, i.e. $FeN_4(O_2)_2$ and FeN_3ClO_2 or $FeN_4(OH)_2$ and FeN_3ClOH respectively, during/after CL preparation.[24] Based on the XAS and XES data discussed here, one cannot distinguish the exact nature of the bonded ligands, where both –OH and $–O_2$ may be formed from water/alcohol solution and from oxygen dissolved in the

solvent, respectively. Moreover, depending on the local pH, the octahedral sites can be formed via adding –OH…H or H-O-H groups in case of mild acidic solutions. No changes in the pre-edge centroid is observed for all the studied materials suggesting that the Fe oxidation state does not change. Moreover, it has been shown for Fe-based minerals of the same oxidation state that the edge position of the O_h structures is typically higher than for D_{4h} / C_{4v}.[22] The analysis of the 1st inflection point (Table 1) of Fe-N-C-based CLs shows a steady edge shift towards higher energies in comparison to the catalyst powders that can be attributed to changes only in Fe coordination at the iron-nitrogen sites. It should be noted, that not all the sites are expected to transform but mostly the surface- and/or sub-surface-located ones that can be easily accessed by water molecules. Additionally, the increase in CN resulting from additional oxygen ligands would influence the white line intensity and lead to sharpening of the XANES features,[21] as observed for the analyzed materials. Changes of the local geometry will also affect the spin state of Fe atoms that one can probe by means of Kβ XES. The Fe Kβ spectrum is governed by 3*p* – 3*d* exchange interactions and is sensitive to the Fe spin state.[18] The Kβ differences Δ between powder and CL shown in the bottom of panels d-f of Figure 2 and Figure S4 exhibit shape that is typical for an increase in total spin.[17] A quantitative analysis of the Kβ spectra can be carried out using the $K\beta_{1,3}$ first moment (M_1), representing the overall blue shift of the emission line, and by the integrated absolute difference (IAD) method.[17] The variations in Kβ-M_1 position of catalyst powders and their CLs are small (Table 1). In case of the IAD analysis, the IAD values are obtained between a given spectrum and a reference spectrum with a known spin state (in this case with spin state = 0) and can be further correlated with the Fe total spin state evolution. The details on the IAD analysis as well as the Kβ spectra of the reference material with zero total spin can be found in the Supporting Information and in Ref. [17]. Independent of the Fe-N-C catalyst, we observe an increase in the IAD

value for the CLs in comparison to the powders. The 4-fold/5-fold → 6-fold transition proposed earlier based on XANES data explains the increase of the IAD value due to a weaker mixing between ligand and metal orbitals in case of O_h coordination in comparison to D_{4h} and C_{4v} as it was discussed in Ref. [17]. Thus, all XAS and XES changes discussed here can be explained with a partial formation of octahedral sites $FeN_4(OH)_2$ and FeN_3ClOH (or in case of oxygen bond formation: $FeN_4(O_2)_2$ and FeN_3ClO_2, respectively) during the CL preparation, where the degree of transition depends on the catalyst initial structure. Specifically, the porphyrin-based materials, Porph/C_{prec} and Porph/C_{cat}, appeared to be more stable towards $–O_2$/–OH bonds formation in comparison to C-PPy and Fe0.5 catalysts where initially present 4-coordinated D_{4h} Fe sites, FeN_4, have higher affinity towards octahedral sites transition.

The analysis of Nafion contribution to the D_{4h} → O_h transition via formation of $–O_2$/–OH bonds is presented in Figure 4, where four parameters were tracked for various Nafion concentrations in the Fe0.5-based CL layers (NCR value): Kβ IAD values, 1st inflection point of XANES, pre-edge and white line intensities. Interestingly, the observed changes are not triggered by Nafion, but rather by the presence of either water and/or isopropanol in the catalyst ink. However, the introduction of Nafion in the catalyst suspension does enhance them reaching a saturation at ca. NCR of 1, probably due to higher water concentration in the CL resulting from the water vapor adsorption by Nafion ionomer clusters formed in the ink.

The formation of iron oxides during Fe-N-C-based CL preparation has been proposed earlier in literature.[16] For this reason, we compared XANES and XES data, where the valence-to-core (VtC) region was also included, of the analyzed catalysts with the ones' recorded on a commercial bulk α-Fe_2O_3 powder (CAS number: 1309-37-1) and also on a home-made Fe nano-oxides (6-8 nm according to the TEM images) deposited on N-doped carbon powder (Fe_2O_3/N-C)[16]. The VtC

spectrum arises from transitions from filled valence orbitals that are dominantly ligand in nature where the low-energy VtC feature, Kβ", is known to be a diagnostic of the ligand bonded to the metal atom.[29] For both iron oxides we observed a similar XANES and VtC signatures (Figure S2 and S3) that is consistent with the spectra available in literature.[30] Particularly, the pre-edge region (Figure S2b) possesses a well-resolved doublet (≈ 7112.8 eV and ≈ 7114.2 eV) and the low energy VtC component, Kβ", at ≈ 7091 eV (Figure S3) arises from Fe-O bonds. None of these features is observed in the spectra of the CL and we thus find no evidence for the formation of a significant amount of iron oxides during the CL preparation. This could be further investigated using wide-angle X-ray scattering coupled with pair-distribution function analysis sensitive to the small clusters and nanoparticles presence, which is beyond the scope of this work.

Table 1. Characteristic parameters of the Kβ XES and XANES spectra obtained for studied catalyst powders and their CLs.

Catalyst	**Form**	**Fe Kβ XES**		**Fe Kβ HERFD XANES**		
		Kβ IAD / arb. units	**Kβ-M_1 / keV**	**pre-edge intensity / arb. units**	**WL intensity / arb. units**	**1st inflection point / keV**
Fe0.5	powder	0.287	7058.8	2.57	21.10	7110.9
	CL: NCR* = 0	0.308	7058.9	1.62	22.87	7111.5
	CL: NCR = 0.25	0.335	7059.1	1.62	23.05	7112.3
	CL: NCR = 0.50	0.335	7059.0	1.37	23.71	7112.8
	CL: NCR = 1.00	0.341	7059.1	1.33	24.32	7113.0
	CL: NCR = 2.00	0.337	7059.0	1.35	24.46	7113.3
C-PPy	powder	0.284	7058.9	2.45	20.48	7110.1
	CL: NCR = 0.23	0.309	7058.9	1.78	22.59	7112.7
Porph/C_{prec}	powder	0.275	7058.7	2.46	21.84	7110.3
	CL: NCR = 0.23	0.302	7058.9	2.27	22.77	7110.4

*NCR = Nafion-to-catalyst ratio

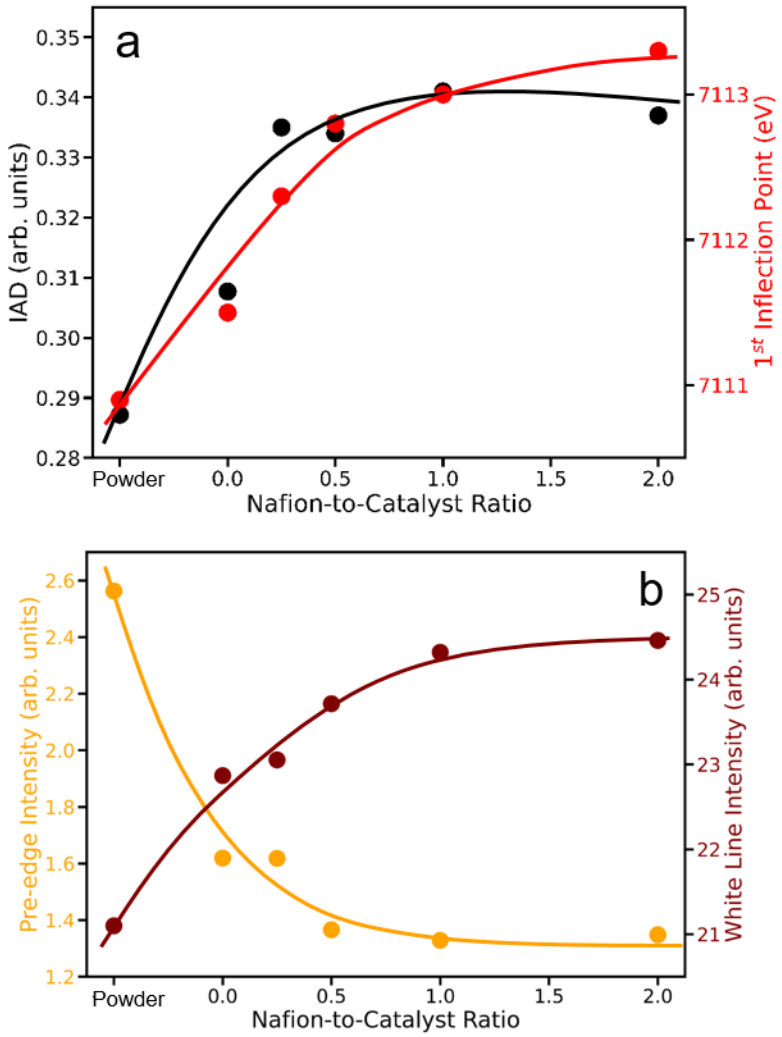

Figure 4. Dependence of Fe Kβ XES (a) and XANES (a, b) spectral parameters on NCR ratio for Fe0.5 catalyst and its electrodes. The lines are provided to guide the reader through the data points and do not possess any physical meaning.

The presence of the solvents (water and alcohols) as well as Nafion binder in the catalyst ink is essential for producing a homogeneous and performing CL for both Pt-based and Pt-free catalysts. In this work, we demonstrated the particularity of the Fe-N-C catalysts, where the FeN_x sites structure partially evolves from square planar (or square pyramidal) to octahedral by adding 1 or 2 $–O_2$ /–OH bond(s) during the electrode preparation procedure and does not fully resemble the one observed in a pristine catalyst powder. While this evolution is universal for Fe-N-C

materials, the magnitude of change varies with the synthesis procedure and consequently with the initial composition of Fe-N-C. In particular, during CL preparation we observe changes in Fe local environment that is induced by adding $–O_2$/–OH ligands that become available through contact with water/alcohol solution. The effect is enhanced by Nafion presence in the catalyst ink. This aspect should be taken into account when discussing the catalyst structure – activity – stability/durability correlation(s) as well as analyzing *in situ*/*operando* measurements performed on these materials, where one should consider the electronic state of Fe in the prepared electrode and not in the catalyst powder.

ASSOCIATED CONTENT

Supporting Information. Details on the XAS/XES measurements and data analysis; catalysis synthesis; CL preparation procedure; additional XANES and XES data.

AUTHOR INFORMATION

Corresponding Author

*Email: viktoriia.saveleva@esrf.fr

Author Contributions

The manuscript was written through contributions of all authors. All authors have given approval to the final version of the manuscript.

Funding Sources

P.T. and U.I.K. acknowledge financial support by the BMBF young researcher group FeNC-StRedO (funding number 03XP0092). F.M., F.J. and K.K. gratefully acknowledge financial

support from the French National Research Agency through the ANIMA (grant number ANR-19-CE05–0039) and the DEEP (grant number ANR-21-CE05-0021) projects.

Notes

Any additional relevant notes should be placed here.

ACKNOWLEDGMENT

We acknowledge the European Synchrotron Radiation Facility for provision of beamtime at ID26 beamline (DOI: 10.15151/ESRF-ES-799089889)

ABBREVIATIONS

CL, catalyst layer; CN, coordination number; GC, glassy carbon; GDL, gas diffusion layer; IAD, integrated absolute difference; MS, Mössbauer spectroscopy; MOF, metal-organic framework; NCR, Nafion-to-catalyst ratio; RT, room temperature; RDE, rotating disc electrode; VtC, valence-to-core; WL, white line; XAS, X-ray absorption spectroscopy; HERFD XANES, high energy resolution fluorescence detected X-ray absorption near edge structure; XES, X-ray emission spectroscopy.

REFERENCES

(1) Deng, X.; Huang, C.; Pei, X.; Hu, B.; Zhou, W. Recent Progresses and Remaining Issues on the Ultrathin Catalyst Layer Design Strategy for High-Performance Proton Exchange Membrane Fuel Cell with Further Reduced Pt Loadings: A Review. *Int. J. Hydrogen Energy* **2022**, *47* (3), 1529–1542. https://doi.org/10.1016/j.ijhydene.2021.10.141.

(2) Kramm, U. I.; Lefèvre, M.; Bogdanoff, P.; Schmeißer, D.; Dodelet, J. P. Analyzing Structural Changes of Fe-N-C Cathode Catalysts in PEM Fuel Cell by Mößbauer Spectroscopy of Complete Membrane Electrode Assemblies. *J. Phys. Chem. Lett.* **2014**, *5*

(21), 3750–3756. https://doi.org/10.1021/jz501955g.

(3) Artyushkova, K.; Workman, M. J.; Matanovic, I.; Dzara, M. J.; Ngo, C.; Pylypenko, S.; Serov, A.; Atanassov, P. Role of Surface Chemistry on Catalyst/Ionomer Interactions for Transition Metal-Nitrogen-Carbon Electrocatalysts. *ACS Appl. Energy Mater.* **2018**, *1*, 68–77. https://doi.org/https://doi.org/10.1021/acsaem.7b00002.

(4) Banham, D.; Kishimoto, T.; Sato, T.; Kobayashi, Y.; Narizuka, K.; Ozaki, J. ichi; Zhou, Y.; Marquez, E.; Bai, K.; Ye, S. New Insights into Non-Precious Metal Catalyst Layer Designs for Proton Exchange Membrane Fuel Cells: Improving Performance and Stability. *J. Power Sources* **2017**, *344*, 39–45. https://doi.org/10.1016/j.jpowsour.2017.01.086.

(5) Li, J.; Jaouen, F. Structure and Activity of Metal-Centered Coordination Sites in Pyrolyzed Metal–Nitrogen–Carbon Catalysts for the Electrochemical Reduction of O2. *Curr. Opin. Electrochem.* **2018**, 1–9. https://doi.org/10.1016/j.coelec.2018.03.039.

(6) Wagner, S.; Auerbach, H.; Tait, C. E.; Martinaiou, I.; Kumar, S. C. N.; Kübel, C.; Sergeev, I.; Wille, H.-C.; Behrends, J.; Wolny, J. A.; Schünemann, V.; Kramm, U. Elucidating the Structural Composition of a Fe-N-C Catalyst by Nuclear and Electron Resonance Techniques. *Angew. Chemie Int. Ed.* **2019**, *58*, 10486–10492. https://doi.org/10.1002/anie.201903753.

(7) Huan, T. N.; Ranjbar, N.; Rousse, G.; Sougrati, M.; Zitolo, A.; Mougel, V.; Jaouen, F.; Fontecave, M. Electrochemical Reduction of CO2 Catalyzed by Fe-N-C Materials: A Structure-Selectivity Study. *ACS Catal.* **2017**, *7* (3), 1520–1525. https://doi.org/10.1021/acscatal.6b03353.

(8) Paul, S.; Kao, Y. L.; Ni, L.; Ehnert, R.; Herrmann-Geppert, I.; van de Krol, R.; Stark, R. W.; Jaegermann, W.; Kramm, U. I.; Bogdanoff, P. Influence of the Metal Center in M−N−C

Catalysts on the CO2 Reduction Reaction on Gas Diffusion Electrodes. *ACS Catal.* **2021**, *11* (9), 5850–5864. https://doi.org/10.1021/acscatal.0c05596.

(9) Jaouen, F.; Proietti, E.; Lefèvre, M.; Chenitz, R.; Dodelet, J.-P. P.; Wu, G.; Chung, H. T.; Johnston, C. M.; Zelenay, P.; Lefevre, M.; Chenitz, R.; Dodelet, J.-P. P.; Wu, G.; Chung, H. T.; Johnston, C. M.; Zelenay, P. Recent Advances in Non-Precious Metal Catalysis for Oxygen-Reduction Reaction in Polymer Electrolyte Fuel Cells. *Energy Environ. Sci.* **2011**, *4* (1), 114–130. https://doi.org/10.1039/c0ee00011f.

(10) Ni, L.; Gallenkamp, C.; Paul, S.; Kübler, M.; Theis, P.; Chabbra, S.; Hofmann, K.; Bill, E.; Schnegg, A.; Albert, B.; Krewald, V.; Kramm, U. I. Active Site Identification in FeNC Catalysts and Their Assignment to the Oxygen Reduction Reaction Pathway by In Situ 57 Fe Mössbauer Spectroscopy . *Adv. Energy Sustain. Res.* **2021**, *2* (2), 2000064. https://doi.org/10.1002/aesr.202000064.

(11) Ebner, K.; Clark, A. H.; Saveleva, V. A.; Smolentsev, G.; Chen, J.; Ni, L.; Li, J.; Zitolo, A.; Jaouen, F.; Kramm, U. I.; Schmidt, T. J.; Herranz, J. Surface-Sensitive and Time-Resolved Potential-Induced Changes in Fe/N/C-Catalysts Studied by In Situ Modulation Excitation X-Ray Absorption Spectroscopy. *Adv. Energy Mater.* **2022**, *12*, 2103699 (14). https://doi.org/10.1002/aenm.202103699.

(12) Boldrin, P.; Malko, D.; Mehmood, A.; Kramm, U. I.; Wagner, S.; Paul, S.; Weidler, N.; Kucernak, A. Deactivation, Reactivation and Super-Activation of Fe-N/C Oxygen Reduction Electrocatalysts: Gas Sorption, Physical and Electrochemical Investigation Using NO and O2. *Appl. Catal. B Environ.* **2021**, *292* (January), 120169. https://doi.org/10.1016/j.apcatb.2021.120169.

(13) Santos, K. T.; Kumar, K.; Dubau, L.; Ge, H.; Berthon-Fabry, S.; Vasconcelos, C. S.; Lima,

F.; Asset, T.; Atanassov, P.; Saveleva, V. A.; Glatzel, P.; Li, X.; Jaouen, F.; Maillard, F. Spontaneous Aerobic Ageing of Fe-N-C Materials and Consequences on Oxygen Reduction Reaction Kinetics. *SSRN* **2022**. https://doi.org/http://dx.doi.org/10.2139/ssrn.4237763.

(14) Chon, G.; Suk, M.; Jaouen, F.; Chung, M. W.; Choi, C. H. Deactivation of Fe-N-C Catalysts during Catalyst Ink Preparation Process. *Catal. Today* **2019**, No. March, 1–7. https://doi.org/10.1016/j.cattod.2019.03.067.

(15) Goellner, V.; Armel, V.; Zitolo, A.; Fonda, E.; Jaouen, F. Degradation by Hydrogen Peroxide of Metal-Nitrogen-Carbon Catalysts for Oxygen Reduction. *J. Electrochem. Soc.* **2015**, *162* (6), H403–H414. https://doi.org/10.1149/2.1091506jes.

(16) Li, J.; Sougrati, M. T.; Zitolo, A.; Ablett, J.; Oguz, I. C.; Mineva, T.; Matanovic, I.; Atanassov, P.; Di Cicco, A.; Kumar, K.; Dubau, L.; Maillard, F.; Jaouen, F. Identification of Durable and Non-Durable FeNx Sites in Fe-N-C Materials for Proton Exchange Membrane Fuel Cells. *Nat. Catal.* **2021**, *4*, 10–19. https://doi.org/https://doi.org/10.1038/s41929-020-00545-2 Identification.

(17) Lafuerza, S.; Carlantuono, A.; Retegan, M.; Glatzel, P. Chemical Sensitivity of Kβ and Kα X-Ray Emission from a Systematic Investigation of Iron Compounds. *Inorg. Chem.* **2020**, *59* (17), 12518–12535. https://doi.org/10.1021/acs.inorgchem.0c01620.

(18) Saveleva, A. V. A.; Ebner, K.; Ni, L.; Klose, D.; Zitolo, A.; Marelli, E.; Li, J.; Medarde, M.; Safonova, O. V; Jaouen, F.; Kramm, U. I.; Thomas, J.; Herranz, J. Potential-Induced Spin Changes in Fe/N/C Electrocatalysts Assessed by in Situ X-Ray Emission Spectroscopy. *Angew. Chemie Int. Ed.* **2021**, *133*, 1–7. https://doi.org/10.1002/anie.202016951.

(19) Kumar, K.; Gairola, P.; Lions, M.; Ranjbar-Sahraie, N.; Mermoux, M.; Dubau, L.; Zitolo,

A.; Jaouen, F.; Maillard, F. Physical and Chemical Considerations for Improving Catalytic Activity and Stability of Non-Precious Metal Oxygen Reduction Reaction Catalysts. *ACS Catal.* **2018**, *8* (12), 11264–11276. https://doi.org/10.1021/acscatal.8b02934.

(20) Scharf, J.; Kübler, M.; David, W.; Wallace, Z.; Kramm, U. I.; Ni, L.; Paul, S. D. Relation between Half-Cell and Fuel Cell Activity and Stability of FeNC Catalysts for the Oxygen Reduction Reaction. *SusMat* **2022**, *2* (5), 630–645. https://doi.org/10.1002/sus2.84.

(21) Guda, A. A.; Guda, S. A.; Martini, A.; Kravtsova, A. N.; Algasov, A.; Bugaev, A.; Kubrin, S. P.; Guda, L. V.; Šot, P.; van Bokhoven, J. A.; Copéret, C.; Soldatov, A. V. Understanding X-Ray Absorption Spectra by Means of Descriptors and Machine Learning Algorithms. *npj Comput. Mater.* **2021**, *7* (1), 1–13. https://doi.org/10.1038/s41524-021-00664-9.

(22) Wilke, M.; Farges, F.; Petit, P. E.; Brown, G. E.; Martin, F. Oxidation State and Coordination of Fe in Minerals: An Fe K-XANES Spectroscopic Study. *Am. Mineral.* **2001**, *86* (5–6), 714–730. https://doi.org/10.2138/am-2001-5-612.

(23) Ramaswamy, N.; Tylus, U.; Jia, Q.; Mukerjee, S. Activity Descriptor Identification for Oxygen Reduction on Nonprecious Electrocatalysts: Linking Surface Science to Coordination Chemistry. *J. Am. Chem. Soc.* **2013**, *135* (41), 15443–15449. https://doi.org/10.1021/ja405149m.

(24) Westre, T. E.; Kennepohl, P.; DeWitt, J. G.; Hedman, B.; Hodgson, K. O.; Solomon, E. I. A Multiplet Analysis of Fe K-Edge 1s → 3d Pre-Edge Features of Iron Complexes. *J. Am. Chem. Soc.* **1997**, *119* (27), 6297–6314. https://doi.org/10.1021/ja964352a.

(25) Boubnov, A.; Roppertz, A.; Kundrat, M. D.; Mangold, S.; Reznik, B.; Jacob, C. R.; Kureti, S.; Grunwaldt, J. D. Towards Advanced Structural Analysis of Iron Oxide Clusters on the Surface of γ-Al 2 O 3 Using EXAFS. *Appl. Surf. Sci.* **2016**, *386*, 234–246.

https://doi.org/10.1016/j.apsusc.2016.05.148.

(26) Osmieri, L.; Wang, G.; Cetinbas, F. C.; Khandavalli, S.; Park, J.; Medina, S.; Mauger, S. A.; Ulsh, M.; Pylypenko, S.; Myers, D. J.; Neyerlin, K. C. Utilizing Ink Composition to Tune Bulk-Electrode Gas Transport, Performance, and Operational Robustness for a Fe–N–C Catalyst in Polymer Electrolyte Fuel Cell. *Nano Energy* **2020**, *75*, 104943. https://doi.org/10.1016/j.nanoen.2020.104943.

(27) Jaouen, F.; Goellner, V.; Lefèvre, M.; Herranz, J.; Proietti, E.; Dodelet, J. P. Oxygen Reduction Activities Compared in Rotating-Disk Electrode and Proton Exchange Membrane Fuel Cells for Highly Active FeNC Catalysts. *Electrochim. Acta* **2013**, *87*, 619–628. https://doi.org/10.1016/j.electacta.2012.09.057.

(28) Pollet, B. G.; Kocha, S. S. Using Ultrasound to Effectively Homogenise Catalyst Inks: Is This Approach Still Acceptable? Recommendations on the Use of Ultrasound for Mixing Catalyst Inks. *Johnson Matthey Technol. Rev.* **2022**, *66* (1), 61–76. https://doi.org/10.1595/205651321X16196162869695.

(29) Pollock, C. J.; Debeer, S. Valence-to-Core X-Ray Emission Spectroscopy: A Sensitive Probe of the Nature of a Bound Ligand. *J. Am. Chem. Soc.* **2011**, *133* (14), 5594–5601. https://doi.org/10.1021/ja200560z.

(30) Glatzel, P.; Mirone, A.; Eeckhout, S. G.; Sikora, M.; Giuli, G. Orbital Hybridization and Spin Polarization in the Resonant 1s Photoexcitations of α- Fe2 O3. *Phys. Rev. B - Condens. Matter Mater. Phys.* **2008**, *77* (11), 1–7. https://doi.org/10.1103/PhysRevB.77.115133.